

Detection of non-ordered central gas motions in a sample of four low surface brightness galaxies^{★,★★} (Research Note)

A. Pizzella¹, D. Tamburro², E. M. Corsini^{1,3}, and F. Bertola¹

¹ Dipartimento di Astronomia, Università di Padova, vicolo dell'Osservatorio 3, 35122 Padova, Italy
e-mail: alessandro.pizzella@unipd.it

² Max-Planck-Institut für Astronomie, Königstuhl 17, 69117 Heidelberg, Germany

³ Scuola Galileiana di Studi Superiori, via VIII Febbraio 2, 35122 Padova, Italy

Received 17 October 2006 / Accepted 15 January 2008

ABSTRACT

Aims. We present integral-field spectroscopy of the ionized gas in the central regions of four galaxies with a low surface brightness disk taken with the Visible Multi Object Spectrograph at the Very Large Telescope and aimed at testing the accuracy in the determination of the central logarithmic slope α of the mass density radial profile $\rho(r) \propto r^\alpha$ in this class of objects.

Methods. For all the sample galaxies we subtracted the best-fit model of gas in circular motions from the observed velocity field and derived the residuals. Only ESO-LV5340200 is characterized by a regular velocity field. We extracted the velocity curves of this galaxy along several position angles, in order to estimate the uncertainty in deriving the central gradient of the total mass density from long-slit spectroscopy.

Results. We report the detection of strong non-ordered motions of the ionized gas in three out of four sample galaxies. The deviations have velocity amplitudes and spatial scales that keep it from being possible to disentangle the cuspy and core density radial profiles.

Key words. galaxies: kinematics and dynamics – galaxies: spiral – galaxies: structure – cosmology: dark matter

1. Introduction

Low surface brightness (LSB) galaxies are defined as disk galaxies with a central face-on brightness fainter than $22.6 B\text{-mag arcsec}^{-2}$. In comparison with high surface brightness (HSB) galaxies, the LSB galaxies have higher mass-to-light ratios and are dominated by the dark matter (DM) even in the central regions (e.g., de Blok et al. 1996; Courteau & Rix 1999; Borriello & Salucci 2001). Therefore, the rotation curves of LSB galaxies are thought to represent an ideal testbed for checking the predictions of N -body simulations in a cold dark matter (CDM) universe, where the mass density radial profile of the DM halos is described by a steep power law $\rho(r) \sim r^\alpha$ (i.e. $\alpha \lesssim -1$, Navarro et al. 1997, 2004; Moore et al. 1999; Diemand et al. 2005).

On the other hand, the observations seem to be inconsistent with the CDM scenario. The DM mass density distribution derived by HI rotation curves of most of LSB galaxies is described by a radial profile with a constant core profile (i.e. $\alpha \approx 0$, McGaugh & de Blok 1998; Salucci 2001). This is also true for the ionized-gas rotation curves (see McGaugh et al. 2001; de Blok et al. 2001; McGaugh et al. 2003). The spatial resolution of these data allows detection of cuspy DM density profiles when they are present, but other authors do find agreement of

the radio (van den Bosch et al. 2000) and optical (Swaters et al. 2003) data with the CDM predictions. Despite this observational effort, a unique answer to the central DM density profile slope has not been found yet.

However, measuring the mass density profile using the gas as a potential tracer in galactic centers may become problematic not only because of the resolution effects. Indeed, the gas can have an intrinsic velocity dispersion and does not necessarily move on perfectly ballistic orbits (Bertola et al. 1995; Cinzano et al. 1999). Moreover, the emissivity distribution of the gas is often clumpy (van den Bosch & Swaters 2001), and the presence of asymmetric and/or decoupled structures could remain undetected in long-slit observations (see Coccato et al. 2005, and references therein). More mundanely, the imperfect centering and orientation of the slit in optical spectroscopy and the beam smearing in radio observations contribute to the total uncertainties on the measured kinematics.

To address all these issues, it is crucial to obtain high-resolution gas kinematics along different axes. Only recently, the two-dimensional velocity field of the ionized gas in LSB galaxies has been measured by means of integral-field units spectroscopy. Simon et al. (2005) studied a sample of low-mass spiral galaxies with a velocity field that can be explained by either a cored or a cuspy radial profile. Kuzio de Naray et al. (2006) observed a sample of LSB galaxies. They find that DM halos with a core of constant mass density provide a better fit to the data compared to those with a density cusp.

In this paper we focus on the intrinsic limitation of the ionized-gas kinematics in tracing the galactic central potential and mass distribution. The work is based on the kinematics in the

* Based on observations carried out at the European Southern Observatory (ESO 71.B-3050).

** Table 2 is only available in electronic form at the CDS via anonymous ftp to [cdsarc.u-strasbg.fr](ftp://cdsarc.u-strasbg.fr) (130.79.128.5) or via <http://cdsweb.u-strasbg.fr/cgi-bin/qcat?J/A+A/482/53>

Table 1. Observing log.

Name	Date	Exp. Time	<i>FWHM</i>
ESO-LV 1860550	07/08 Apr. 2003	2 × 45 min	0′.4/0′.6
ESO-LV 3520470	31 Jul. 2003	1 × 45 min	N/A
ESO-LV 4000370	24 Aug. 2003	1 × 45 min	0′.5
ESO-LV 5340200	28/29 Jun. 2003	2 × 45 min	0′.7/0′.6

center of four galaxies with an LSB disk measured by integral-field spectroscopy. The observations and data reduction are described in Sect. 2. The measurement and analysis of the kinematics and distribution of the ionized gas are discussed in Sect. 3. The results are given in Sect. 4. Finally, the conclusions are presented in Sect. 5.

2. Observations and data reduction

The sample galaxies were selected among those observed by [McGaugh et al. \(2001\)](#) and [Pizzella et al. \(2008a\)](#) to have an LSB disk and measured ionized-gas kinematics with long-slit spectroscopy. Their main properties are reported in Fig. 1.

The integral-field spectroscopic observations were carried out with the Very Large Telescope (VLT) at the European Southern Observatory (ESO) in Paranal (Chile) in 2003. The Unit Telescope 3 was used in combination with the Visible Multi Object Spectrograph (VIMOS) in the Integral Field Unit (IFU) configuration. The field of view of the four VIMOS channels (Q1-Q4) was $13'' \times 13''$ and was projected onto a microlens array. This was coupled to optical fibers that were rearranged on a linear set of microlenses to produce an entrance pseudoslit to the spectrograph. The pseudoslit generated a total of 1600 spectra covering the field of view with a spatial resolution of 0′.33 per fiber. Each channel was equipped with the HR_orange high-resolution ($R \sim 2500$) grism and a thinned and back-illuminated EEV44 CCD with 2048×4096 pixels of $15 \times 15 \mu\text{m}^2$. The wavelength range between 5250 and 7450 Å was covered with a reciprocal dispersion of $0.65 \text{ \AA pixel}^{-1}$. The observing log and values of the full width at half maximum (*FWHM*) of the seeing as measured by the ESO Differential Image Meteor Monitor are reported in Table 1.

For each VIMOS channel all the spectra were traced, identified, bias-subtracted, flatfield-corrected, corrected for relative fiber transmission, and wavelength-calibrated using the routines of the VIPGI pipeline ([Scodreggio et al. 2005](#)). The cosmic rays and bad pixels were identified and cleaned using our routines developed under the IDL environment¹. We checked and corrected the wavelength rebinning by measuring the difference between the measured and predicted wavelengths for the 23 brightest night-sky emission lines in the observed spectral range ([Osterbrock et al. 1996](#)). The rms of the differences was 0.08 \AA (Q1), 0.05 \AA (Q2), 0.05 \AA (Q3), and 0.07 \AA (Q4), corresponding to an accuracy in wavelength calibration of 3 km s^{-1} in the observed spectral range. The intensity of the night-sky emission lines was used to correct for the different relative transmission of the VIMOS channels. The width of the night-sky emission lines was used to estimate the instrumental line width. We measured $FWHM = 1.86 \pm 0.19 \text{ \AA}$ (Q1), $1.81 \pm 0.19 \text{ \AA}$ (Q2), $1.88 \pm 0.14 \text{ \AA}$ (Q3), and $1.84 \pm 0.14 \text{ \AA}$ (Q4), corresponding to an instrumental velocity dispersion $\sigma_{\text{inst}} = 36 \text{ km s}^{-1}$.

¹ The Interactive Data Language is a product of Research Systems, Inc. (RSI).

3. Analysis

The ionized-gas kinematics was measured by fitting the brightest emission lines in the galaxy spectra. They were the $H\alpha$ and [N II] $\lambda 6583$ lines for ESO-LV 1860550 and ESO-LV 4000370, $H\alpha$ and [S II] $\lambda 6716$ lines for ESO-LV 3520470, and $H\alpha$ line for ESO-LV 5340200. A Gaussian profile and a straight line were fitted to each emission line and its adjacent continuum, respectively. The lines were assumed to share a common centroid velocity and a common velocity width. The heliocentric correction was applied to the fitted line-of-sight velocities. They were not corrected for the galaxy inclination. The fitted line-of-sight velocity dispersions were corrected for the instrumental velocity dispersion. No flux calibration was performed. The resulting kinematics of the ionized gas, as well as the intensity maps of the stellar continuum and fitted emission lines, are plotted in Fig. 1. The resulting line-of-sight heliocentric velocities and velocity dispersions are listed in Table 2.

[McGaugh et al. \(2001\)](#) measured the gas kinematics along the major axis of ESO-LV 3520470. [Pizzella et al. \(2008a\)](#) measured the gas kinematics along several axes of the remaining three galaxies. A comparison with these datasets was performed to assess the accuracy and reliability of our measurements. We extracted from our two-dimensional velocity fields the velocity curves along the same axes as observed by [McGaugh et al. \(2001\)](#) and [Pizzella et al. \(2008a\)](#) mimicking their instrumental setup. For all the galaxies we found agreement with the errors between the velocity curves extracted from the two-dimensional velocity fields and the long-slit measurements. The best match was found for the major-axis rotation curve of ESO-LV 5340200 (Fig. 2). The largest deviations ($\Delta v \approx 40 \text{ km s}^{-1}$) were observed along a diagonal axis ($PA = 165^\circ$) of ESO-LV 1860550 (Fig. 2), and they can be attributed to the different point spread functions and spatial samplings of the two datasets.

For each galaxy, we fitted the observed velocity field with the model of a thin disk of rotating gas to investigate the presence of non-circular and non-ordered motions. They limit the accuracy of the mass density distribution derived from the available kinematics. The model of the gas velocity field is generated assuming that the ionized-gas component is moving onto circular orbits in an infinitesimally thin disk with a negligible velocity dispersion. We assume that the circular velocity v_{disk} at a given radius r of the gaseous disk is

$$v_{\text{disk}}(r) = v_{\infty} \left[1 - \frac{h}{r} \arctan \frac{r}{h} \right]^{\frac{1}{2}}, \quad (1)$$

where v_{∞} and h are the asymptotic velocity and a scale radius, respectively. Following [Cocato et al. \(2007\)](#), the ionized-gas velocity measured along the line of sight at a given sky point (x, y) is

$$v_{\text{los}}(x, y) = v_{\text{disk}}(r) \sin i \cos \phi + v_{\text{sys}}, \quad (2)$$

where v_{sys} is the systemic velocity of the galaxy. The anomaly ϕ is measured on the disk plane and it is defined by

$$\cos \phi = [(x - x_0) \cos \theta + (y - y_0) \sin \theta] / R, \quad (3)$$

where (x_0, y_0) , i , and θ are the coordinates of the center, inclination, and position angle of the line of nodes of the gaseous disk, respectively. The parameters of our model are the asymptotic velocity, velocity scale radius, and position angle of the gaseous disk, and the systemic velocity of the galaxy. The disk inclination was not fitted because the field of view was too small to properly constrain it. We adopted the inclination given by

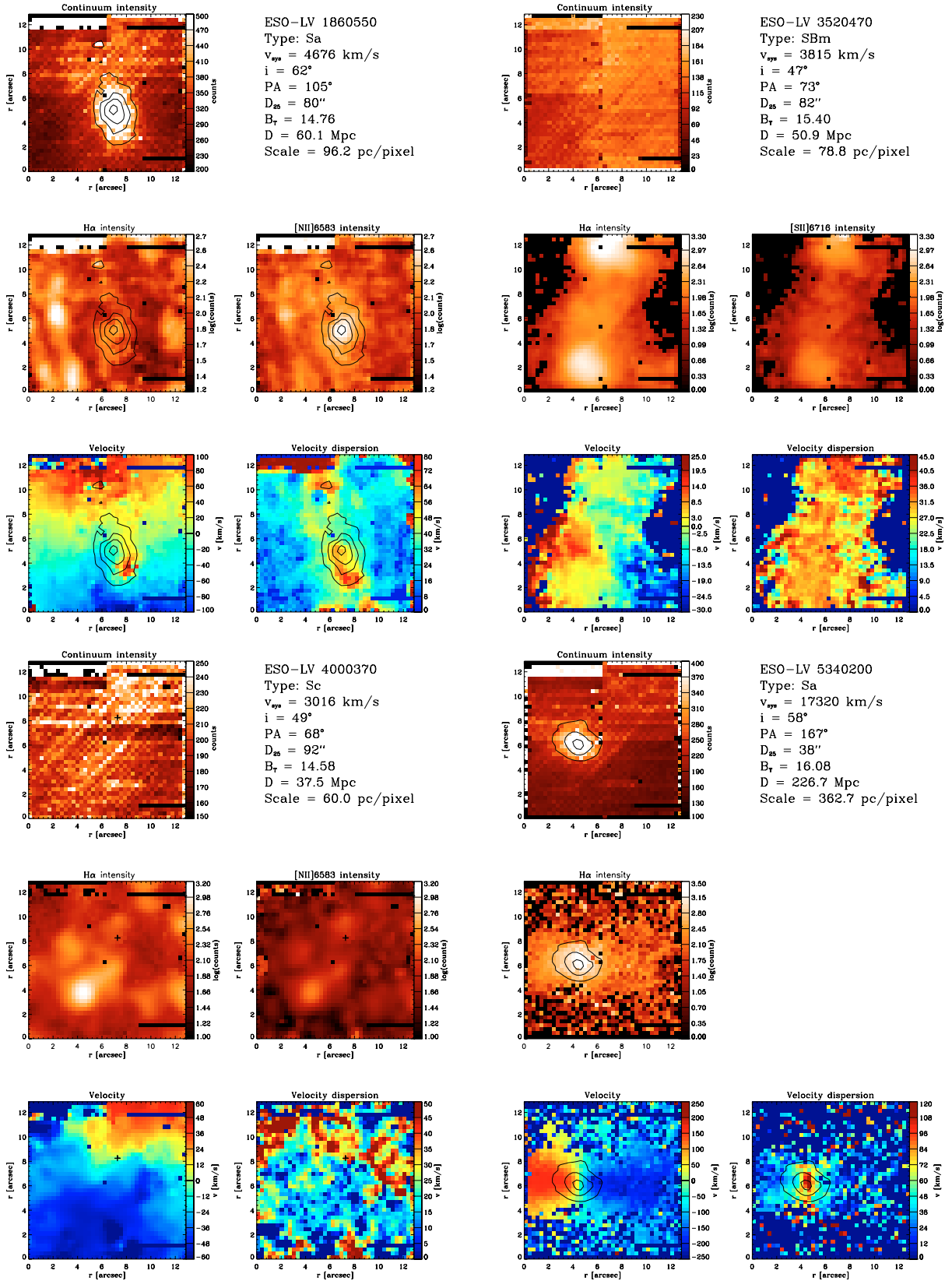


Fig. 1. Maps of the distribution and kinematics of the sampled gas for the sample galaxies. East is up and north is right. The ranges are indicated on the right of each panel. *Upper panel:* reconstructed image of the galaxy obtained by integrating the stellar continuum between 5728 and 5758 Å. *Middle left panel:* H α intensity map. *Middle right panel:* [N II] λ 6583 (or [S II] λ 6716) intensity map. *Lower left panel:* heliocentric line-of-sight velocity without applying any correction for galaxy inclination. *Lower right panel:* line-of-sight velocity dispersion corrected for instrumental velocity dispersion. The morphological classification, inclination, majoraxis position angle, diameter of the 25 B -mag arcsec $^{-2}$ isophote, and total blue magnitude are taken from [Lauberts & Valentijn \(1989, ESO-LV\)](#). The systemic velocities are from this paper. The distances are derived from the systemic velocities corrected to the CMB reference frame following [Fixsen et al. \(1996\)](#) and assuming $H_0 = 75$ km s $^{-1}$ Mpc $^{-1}$.

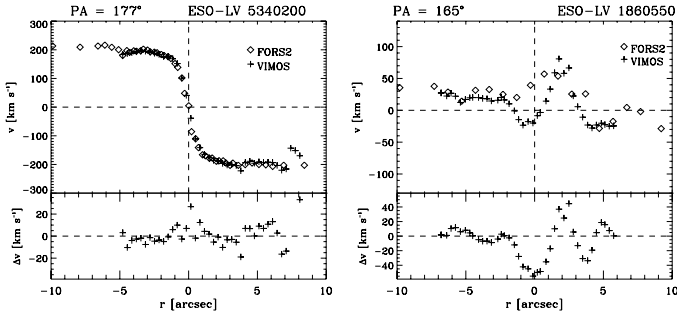


Fig. 2. The rotation curves measured in this paper (*crosses*) along the majoraxis of ESO-LV 5340200 (*left panel*) and a diagonal axis of ESO-LV 1860550 (*right panel*) compared with those obtained from long-slit spectra by Pizzella et al. (2008a, *diamonds*).

the ESO-LV catalog (Fig. 1). The center of the gaseous disk was assumed to be coincident with the position of the intensity peak of the stellar continuum of the reconstructed image for ESO-LV 1860550 and ESO-LV 5340200 (Fig. 1). No intensity peak was observed for ESO-LV 3520470 and ESO-LV 4000370. Therefore, for these galaxies x_0 and y_0 were left as free parameters. The best-fitting parameters were obtained by iteratively fitting a model velocity field to the observed one using a non-linear least-squares minimization method. It is based on the robust Levenberg-Marquardt method implemented by Moré et al. (1980). The actual computation was done using the MPFIT algorithm under the IDL environment. The seeing effects were taken into account by convolving the model with a Gaussian kernel with an *FWHM* as given in Table 1. Finally, the model was compared to the observed velocity field excluding bad or dead fibers. We were not able to construct any reliable disk model for ESO-LV 3520470, because its velocity field turned out to be very irregular.

Assuming a spherical mass distribution, the mass density profile is given by

$$\rho(r) = \frac{1}{4\pi G} \left[2 \frac{v_c}{r} \frac{dv_c}{dr} + \left(\frac{v_c}{r} \right)^2 \right], \quad (4)$$

where v_c is the circular velocity (e.g., de Blok et al. 2001; Swaters et al. 2003). To avoid possible biases, we derived v_c by deprojecting the line-of-sight velocities v_{los} measured along different axes without adopting any parametric function (e.g., Eq. (1)) to describe the velocity field. Finally, we fitted the resulting mass density profiles with a power law $\rho(r) \sim r^\alpha$. The logarithmic slope α was derived excluding the data points inside the seeing disk (Table 1). ESO-LV 5340200 was the only sample galaxy with a velocity field suitable for such a kind of analysis. The gas velocity fields of the other three galaxies were dominated by non-circular and non-ordered motions.

4. Results

4.1. ESO-LV 1860550

The field of view covers $3.8 \times 3.8 \text{ kpc}^2$ at the galaxy distance. The intensity and kinematic maps derived from the two exposures available for this galaxy are in agreement. The intensity maps of the $\text{H}\alpha$ and $[\text{N II}] \lambda 6583$ lines are shown in Fig. 1. They unveil the presence in the center of the field of view of a region with a size of about $7'' \times 14''$ and oriented along the galaxy major axis, where $I([\text{N II}] \lambda 6583)/I(\text{H}\alpha) \geq 2$. At larger radii the ratio drops to 0.7 and the distribution of the ionized gas becomes

patchier with the emission regions aligned in a sort of spiral-arm structure. We argued that these features are due to gas exhaustion by massive stellar formation and to shocks induced by radiation and winds, as found in the center of NGC 7331 by Battaner et al. (2003).

The velocity field exhibits the overall shape of a rotating disk (Fig. 1). However, there are signatures of non-ordered motions in the inner few arcsec. They are clearly visible in the residual map (Fig. 3) obtained by subtracting the circular velocity model from the observed velocity field. In particular, there is a structure receding with $v \simeq 120 \text{ km s}^{-1}$, which is characterized by the highest velocity dispersion measured in the frame ($\sigma \simeq 80 \text{ km s}^{-1}$). It is located in the southeastern quadrant of the field of view at about $3''$ from the galactic center. In the same region, we measured a narrow ($\sigma \simeq 50 \text{ km s}^{-1}$) $\text{H}\alpha$ absorption line. It is likely that it is due to a (relatively cold) hydrogen cloud, which is located between the observer and the galaxy and falling towards the galactic center. This region was masked in calculating the circular velocity model to minimize systematic errors. Except for such a remarkable feature, the velocity dispersion field is regular and symmetric. The velocity dispersion peaks at about 60 km s^{-1} in the very center and then it decreases outwards. The asymmetry and irregularity of the observed velocity field, which are possibly due to an ongoing acquisition event, prevented us from deriving the radial profile of the mass density.

4.2. ESO-LV 3520470

The field of view covers $3.2 \times 3.2 \text{ kpc}^2$ at the galaxy distance. We excluded the $[\text{N II}] \lambda 6583$ line in measuring the kinematics and distribution of the ionized-gas in ESO-LV 3520470, since it blended with a night-sky emission line. The $\text{H}\alpha$ and $[\text{S II}] \lambda 6716$ intensity maps show that the emitting regions are aligned along the galaxy major axis (Fig. 1). The ionized-gas distribution is characterized by three prominent blobs: a fainter one in the galactic center and two brighter ones on the two sides.

There is no velocity gradient along the galaxy's major axis. This is consistent with the long-slit observations in the same wavelength range as in McGaugh et al. (2001). They found that the gas rotation is very low ($v \leq 10 \text{ km s}^{-1}$) out to $20''$. We measured a $\Delta v \simeq 50 \text{ km s}^{-1}$ over a radial range of $16''$ (corresponding to about 4 kpc) in a direction close to the galaxy minor axis ($\text{PA} = 160^\circ$). The misaligned velocity gradient is not associated to any feature of the intensity maps, since its center of symmetry is offset by about $2''$ westward with respect to the central intensity peak. These features could be interpreted as due to the presence of a kinematically-decoupled component, similar to the inner polar disks found in a number of early-type disk galaxies (Corsini et al. 2003; Coccato et al. 2005; Sil'Chenko 2006). After masking the central region, negligible rotation velocities are observed. Therefore, we were not able to find the kinematic center, and the radial profile of the mass density was not derived.

4.3. ESO-LV 4000370

The field of view covers $2.4 \times 2.4 \text{ kpc}^2$ at the galaxy distance. The center of the field does not correspond to the kinematic center, which is located in the northeastern quadrant. It is marked with a cross in Fig. 1. The $\text{H}\alpha$ and $[\text{S II}] \lambda 6716$ intensity maps show a clumpy distribution of the ionized gas. An intensity peak was observed in the southwestern quadrant at about $6''$ from the galactic center, which is characterized by a low emission intensity.

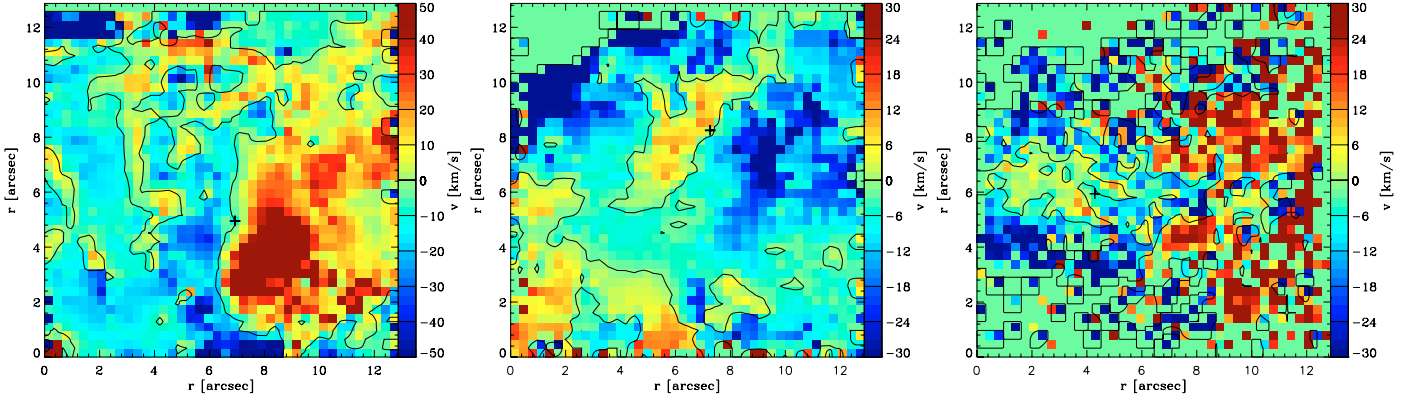


Fig. 3. Map of the velocity residuals of ESO-LV 1860550 (*left panel*), ESO-LV 4000370 (*central panel*), and ESO-LV 5340200 (*right panel*) after subtracting the best-fit circular velocity field. A cross indicates the kinematic center.

The velocity field, although not entirely visible, is not characterized by the expected pattern for a regular rotating disk. In fact, it displays an S-shaped distortion in the nucleus and rotation around the galaxy minor axis. The central kinematically-decoupled component is seen in the residual map (Fig. 3) obtained by subtracting the circular velocity model from the observed velocity field, after masking the central regions. It has a size of about $4''$ (corresponding to 0.7 kpc) and a $\Delta v \simeq 60$ km s $^{-1}$. Its position angle is $PA = 150^\circ$, whereas the position angle of the galaxy’s major axis is $PA = 68^\circ$. The velocity dispersion reaches its maximum value of about 45 km s $^{-1}$ in the center, and it is mildly correlated with the $I([\text{N II}]\lambda 6583)/I(\text{H}\alpha)$ ratio. Its value is about 1 in the very center and it falls to less than 0.5 at larger radii. Due to the poor centering of the galaxy on the field of view, the small number of data points did not allow the central mass density distribution to be derived for this object.

4.4. ESO-LV 5340200

This is the farthest galaxy of the sample. It was included in our list due to the wrong systemic velocity ($cz = 3551$ km s $^{-1}$) reported in the ESO-LV catalog. We measured $v_{\text{sys}} = 17320$ km s $^{-1}$ and derived a distance of 227 Mpc. Therefore, the field of view covers 14×14 kpc 2 . The two exposures available for this galaxy differ in the telescope pointing. The intensity and kinematic maps derived from them agree, which ensures that the data reduction was successfully performed. We excluded the $[\text{N II}]\lambda 6583$ line in measuring the kinematics and distribution of the ionized-gas in ESO-LV 5340200, since it blended with two night-sky emission lines. The distribution of the ionized gas seen in the $\text{H}\alpha$ intensity map is similar to that of the stars shown in the reconstructed image of the stellar continuum (Fig. 1).

The velocity field of the ionized gas exhibits the overall shape of a rotating disk (Fig. 1). ESO-LV 5340200 has the most regular field of the sample galaxies. The rms is 8 km s $^{-1}$ in the central 2×3 kpc 2 of the residual image obtained by subtracting the circular velocity model from the observed velocity field (Fig. 3). Only kinematic sub-structures with a size smaller than 0.5 kpc remain undetected. For a comparison, we measured the rms in the residual map of ESO-LV 1860550 after rebinning it to the spatial sampling of ESO-LV 5340200. We found an rms of 25 km s $^{-1}$ (26 km s $^{-1}$ before the rebinning). The velocity dispersion is about 40 km s $^{-1}$. Only in the central fibers does it peak at a maximum value of about 120 km s $^{-1}$, due to the

combined effect of the limited spatial resolution and sharp velocity gradient.

Since the ionized gas of ESO-LV 5340200 is characterized by ordered motions, we used its velocity field as a test case for studying the typical uncertainties in estimating the mass density profile by means of long-slit spectroscopy. We divided the disk into five 22.5° -wide wedges. The first wedge is oriented along the line of nodes, two wedges are oriented along directions that are offset $\pm 22.5^\circ$ from the line of nodes, and the last two wedges are oriented along directions offset $\pm 45^\circ$ from the line of nodes. According to galaxy inclination and orientation, the wedges are oriented on the sky plane along directions which are $\pm 12.4^\circ$ and $\pm 27.9^\circ$ from the galaxy kinematic major axis ($PA = 177^\circ$). We extracted the velocity curve in each wedge of the two-dimensional velocity field. Ten velocity curves were derived, since the approaching and receding sides of the galaxy were independently considered. For each curve, we computed the term dv_c/dr on adjacent points. The density profiles were thus derived from Eq. (4) and plotted in Fig. 4. The logarithmic slope $\alpha = 1.2 \pm 0.3$ was determined at a distance from the center equal to the seeing disk size, where we were confident that the data were not affected by beam smearing effects. The size of the deprojected seeing disk increases for directions drifting away from the major axis as shown in Fig. 4. The scatter in the measurements is caused by random errors in the α determination. We did not find any trend with the position angle, as we would expect if the non-circular motions induced by a triaxial component were present. It is worth noticing that the galaxy distance and the presence of a bright bulge (Pizzella et al. 2008a) do not allow us to derive the mass density distribution of the DM component without applying a full dynamical model (Corsini et al. 1999; Pignatelli et al. 2001, e.g.). The velocity field of ESO-LV 5340200 is different from those of LSB galaxies analyzed in measuring the central content and distribution of DM to address the core/cusp problem (e.g., de Blok et al. 2001; McGaugh et al. 2003; Kuzio de Naray et al. 2006). In particular, the central velocity gradients of ESO-LV 5340200 was derived with larger uncertainties, and therefore the value of 0.3 can be considered an upper limit to the typical uncertainty in the estimation of logarithmic slope α .

5. Discussion and conclusions

The results of the study of the sample galaxies can be summarized in two remarkable aspects, concerning the presence of non-ordered motions of the ionized gas and the uncertainties of

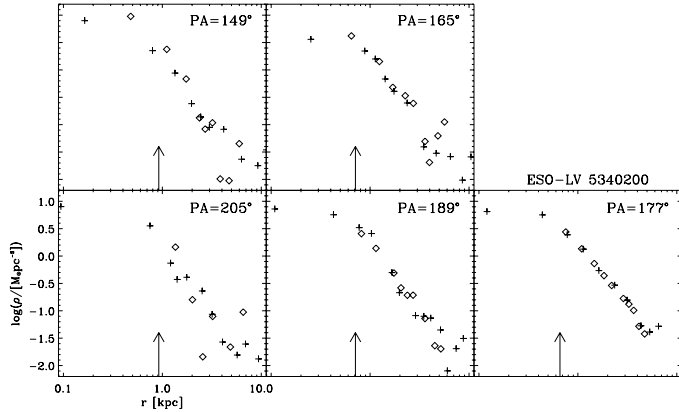


Fig. 4. The mass density profiles along the major ($PA = 177^\circ$) and four diagonal axes of ESO-LV 5340200. In each panel the diamonds and crosses correspond to data measured along the approaching and receding side of the galaxy, respectively. The arrow marks the size of the seeing disk.

recovering the logarithmic slope of the radial profile of the mass density in galaxies with regular kinematics.

In three objects we found the evidence for both non-ordered motions and kinematically-decoupled components. ESO-LV 3520470 and ESO-LV 4000370 host a small (~ 1 kpc) structure that is rotating around the galaxy minor axis. In ESO-LV 1860550 we found the evidence of a gaseous component infalling toward the galactic center. There is no strong correlation between the distribution and kinematics of the ionized-gas of these galaxies and their starlight distribution. Indeed, there is no hint of the decoupled components in broad-band images (see Pizzella et al. 2008a).

These kinematic disturbances seriously affect the determination of the radial profile of the mass density. In fact, the typical sizes of these features (0.5–1 kpc) are comparable to the radial range where the differences between the core and cuspy density radial profiles are expected to be observed. Their velocity amplitudes ($30\text{--}50$ km s $^{-1}$) are also close to both the observed rotation velocities and velocity differences inferred by the different mass density profiles. The majority of previous studies on the central mass distribution of LSB galaxies were based on long-slit spectroscopy, where the presence of kinematic irregularities could have been undetected. Non-circular motions are a common phenomenon in inner regions of disk galaxies. Indeed, Coccato et al. (2004) find that about 50% of the unbarred bright galaxies show strong off-plane and non-circular gas motions in their centers.

ESO-LV 5340200 was the only sample galaxy characterized by a regular velocity field. It was too distant to recover the mass density radial profile in the central kpc with the desired accuracy. However, it represented a good testbed for estimating the uncertainties of the measurement of the central velocity gradient. This is crucial in deriving the logarithmic slope α of the mass density radial profile in objects displaying regular kinematics. We found $\alpha = 1.2 \pm 0.3$. The error was obtained by fitting a power law to the density distribution derived from the different rotation curves extracted along several position angles. Therefore, it represents a good estimate of the scatter obtained by deriving α using the gas kinematic measured from long-slit spectroscopy. On the other hand, the central velocity gradient of ESO-LV 5340200 is larger than for typical LSB galaxies. We concluded the error

we derived can be considered an upper limit to the typical uncertainty in the estimation of logarithmic slope of the mass density. Although it may be substantially reduced with the analysis of the full two-dimensional velocity field (Simon et al. 2005; Kuzio de Naray et al. 2006), the presence of non-circular and non-ordered gas motion remains an unresolved issue. A way to circumvent it is to use the stellar kinematics. The measurement of the stellar line-of-sight velocity distribution (Pizzella et al. 2008a) allows reliable mass models to be built to provide a valid alternative to the usual gas-based mass distribution determinations (Pizzella et al. 2008b; Magorrian et al. 2008).

Acknowledgements. The data published in this paper were reduced using the VIMOS Interactive Pipeline and Graphical Interface (VIPGI) designed by the VIRMOS Consortium. We thank Bianca Garilli for her support in using VIPGI and hospitality at the INAF-IASF Milano. This work was made possible through grants PRIN 2005/32 by Istituto Nazionale di Astrofisica (INAF) and CPDA068415/06 by Padua University.

References

- Battaner, E., Mediavilla, E., Gujarro, A., Arribas, S., & Florido, E. 2003, *A&A*, 401, 67
- Bertola, F., Cinzano, P., Corsini, E. M., Rix, H., & Zeilinger, W. W. 1995, *ApJ*, 448, L13
- Borriello, A., & Salucci, P. 2001, *MNRAS*, 323, 285
- Cinzano, P., Rix, H.-W., Sarzi, M., et al. 1999, *MNRAS*, 307, 433
- Coccato, L., Corsini, E. M., Pizzella, A., et al. 2004, *A&A*, 416, 507
- Coccato, L., Corsini, E. M., Pizzella, A., & Bertola, F. 2005, *A&A*, 440, 107
- Coccato, L., Corsini, E. M., Pizzella, A., & Bertola, F. 2007, *A&A*, 465, 777
- Corsini, E. M., Pizzella, A., Sarzi, M., et al. 1999, *A&A*, 342, 671
- Corsini, E. M., Pizzella, A., Coccato, L., & Bertola, F. 2003, *A&A*, 408, 873
- Courteau, S., & Rix, H. 1999, *ApJ*, 513, 561
- de Blok, W. J. G., McGaugh, S. S., & van der Hulst, J. M. 1996, *MNRAS*, 283, 18
- de Blok, W. J. G., McGaugh, S. S., Bosma, A., & Rubin, V. C. 2001, *ApJ*, 552, L23
- Diemand, J., Zemp, M., Moore, B., Stadel, J., & Carollo, C. M. 2005, *MNRAS*, 364, 665
- Fixsen, D. J., Cheng, E. S., Cottingham, D. A., et al. 1996, *ApJ*, 470, 63
- Kuzio de Naray, R., McGaugh, S. S., de Blok, W. J. G., & Bosma, A. 2006, *ApJS*, 165, 461
- Lauberts, A., & Valentijn, E. A. 1989, *The Surface Photometry Catalogue of the ESO-Uppsala Galaxies (European Southern Observatory, Garching)*
- Magorrian, J., Sarzi, M., Corsini, E. M., et al. 2008, *MNRAS*, in preparation
- McGaugh, S. S., & de Blok, W. J. G. 1998, *ApJ*, 499, 41
- McGaugh, S. S., Rubin, V. C., & de Blok, W. J. G. 2001, *AJ*, 122, 2381
- McGaugh, S. S., Barker, M. K., & de Blok, W. J. G. 2003, *ApJ*, 584, 566
- Moore, B., Quinn, T., Governato, F., Stadel, J., & Lake, G. 1999, *MNRAS*, 310, 1147
- Moré, J. J., Garbow, B. S., & Hillstrom, K. E. 1980, *User guide for MINPACK-1 (Argonne National Laboratory Report ANL-80-74)*
- Navarro, J. F., Frenk, C. S., & White, S. D. M. 1997, *ApJ*, 490, 493
- Navarro, J. F., Hayashi, E., Power, C., et al. 2004, *MNRAS*, 349, 1039
- Osterbrock, D. E., Fulbright, J. P., Martel, A. R., et al. 1996, *PASP*, 108, 277
- Pignatelli, E., Corsini, E. M., Vega Beltrán, J. C., et al. 2001, *MNRAS*, 323, 188
- Pizzella, A., Corsini, E., Sarzi, M., et al. 2008a, *MNRAS*, submitted
- Pizzella, A., Corsini, E. M., Sarzi, M., Magorrian, J., & Bertola, F. 2008b, in *Formation and Evolution of Galaxies*, ed. J. G. Funes, & S. J. E. M. Corsini (ASP, San Francisco), in press
- Salucci, P. 2001, *MNRAS*, 320, L1
- Scodreggio, M., Franzetti, P., Garilli, B., et al. 2005, *PASP*, 117, 1284
- Sil'chenko, O. K. 2006, in *Astrophysical Disks*, ed. A. V. Fridman, M. Y. Marov, & I. G. Kovalenko (Dordrecht: Springer), *ASSL Vol. 337*, 275
- Simon, J. D., Bolatto, A. D., Leroy, A., Blitz, L., & Gates, E. L. 2005, *ApJ*, 621, 757
- Swaters, R. A., Verheijen, M. A. W., Bershady, M. A., & Andersen, D. R. 2003, *ApJ*, 587, L19
- van den Bosch, F. C., & Swaters, R. A. 2001, *MNRAS*, 325, 1017
- van den Bosch, F. C., Robertson, B. E., Dalcanton, J. J., & de Blok, W. J. G. 2000, *AJ*, 119, 1579